The influence of propagating and evanescent waves on the focusing properties of zone plate structures

Jia-Han Li*, Yi-Wei Cheng, Yu-Cheng Chue, Chih-Hung Lin, and Tony Wen-Hann Sheu

Department of Engineering Science and Ocean Engineering, National Taiwan University, No. 1, Sec. 4, Roosevelt Road, Taipei 10617, Taiwan

*jiahan@ntu.edu.tw

Abstract: The field properties of Fresnel zone plates with wavelength-scale focal distances were numerically investigated using the finite-difference time-domain method. The fields in the focal planes are analyzed using the angular spectrum representation, and the components of the propagating and evanescent waves are reconstructed. It was found that, in the focal plane of silver zone plates, there were more evanescent waves and the propagating waves occurred at higher spatial frequencies relative to glass zone plates. The propagating and evanescent wave components vary with the material and the number of zones in the zone plate structures. Our findings suggest that more evanescent waves and higher spatial frequency components of propagating waves can shape the field and obtain a smaller focus.

OCIS codes: (240.6680) Surface plasmons; (050.1965) Diffractive lenses.

References and links

1. E. Abbe, "Beiträge zur Theorie des Mikroskops und der mikroskopischen Wahrnehmung," Archiv für Mikroskopische Anatomie **9**(1), 413–468 (1873).
2. J. B. Pendry, "Negative Refraction Makes a Perfect Lens," Phys. Rev. Lett. **85**(18), 3966–3969 (2000).
3. D. R. Smith, J. B. Pendry, and M. C. K. Wiltshire, "Metamaterials and Negative Refractive Index," Science **305**(5685), 788–792 (2004).
4. R. Hillenbrand, T. Taubner, and F. Keilmann, "Phonon-enhanced light-matter interaction at the nanometre scale," Nature **418**(6894), 159–162 (2002).
5. W. Srituravanich, L. Pan, Y. Wang, C. Sun, D. B. Bogy, and X. Zhang, "Flying plasmonic lens in the near field for high-speed nanolithography," Nature Nanotechnology **3**, 733–737 (2008).
6. N. Fang, H. Lee, C. Sun, and X. Zhang, "Sub-Diffraction-Limited Optical Imaging with a Silver Superlens," Science **308**(5721), 534–537 (2005).
7. Z. Liu, H. Lee, Y. Xiong, C. Sun, and X. Zhang, "Far-Field Optical Hyperlens Magnifying Sub-Diffraction-Limited Objects," Science **315**(5819), 1686 (2007).
8. G. Lerosey, J. de Rosny, A. Tourin, and M. Fink, "Focusing Beyond the Diffraction Limit with Far-Field Time Reversal," Science **315**(5815), 1120–1122 (2007).
9. J. B. Pendry, "Time Reversal and Negative Refraction," Science **322**(5898), 71–73 (2008).
10. J. H. Rice, "Beyond the diffraction limit: far-field fluorescence imaging with ultrahigh resolution," Mol. BioSyst. **3**, 781–793 (2007).
11. R. Merlin, "Radiationless electromagnetic interference: evanescent-field interference lenses and perfect focusing," Science **317**(5840), 927–929 (2007).
12. F. M. Huang and N. I. Zheludev, "Super-Resolution without Evanescent Waves," Nano Lett. **9**(3), 1249–1254 (2009).

#116967 - $15.00 USD Received 9 Sep 2009; accepted 24 Sep 2009; published 28 Sep 2009

13. A. Grbic, L. Jiang, and R. Merlin, "Near-Field Plates: Subdiffraction Focusing with Patterned Surfaces," Science **320**(5875), 511–513 (2008).
14. A. Grbic and R. Merlin, "Near-Field Focusing Plates and Their Design," IEEE Trans. Antennas Propag. **56**(10), 3159–3165 (2008).
15. L. E. Helseth, "The almost perfect lens and focusing of evanescent waves," Opt. Commun. **281**(8), 1981–1985 (2008).
16. L. E. Helseth, "Radiationless electromagnetic interference shaping of evanescent cylindrical vector waves," Phys. Rev. A **78**(1), 013,819 (2008).
17. Y. Fu, W. Zhou, L. E. N. Lim, C. L. Du, and X. G. Luo, "Plasmonic microzone plate: Superfocusing at visible regime," Appl. Phys. Lett. **91**(6), 061,124 (2007).
18. Y. Fu, W. Zhou, and L. E. N. Lim, "Near-field behavior of zone-plate-like plasmonic nanostructures," J. Opt. Soc. Am. A **25**, 238–249 (2008).
19. Y. Fu, W. Zhou, and L. E. N. Lim, "Propagation properties of plasmonic micro-zone plates with and without fractals," Appl. Phys. B **90**(3-4), 421–425 (2008).
20. R. G. Mote, S. F. Yu, B. K. Ng, W. Zhou, and S. P. Lau, "Near-field focusing properties of zone plates in visible regime - New insights," Opt. Exp. **16**(13), 9554–9564 (2008).
21. F. L. Pedrotti, S. J. and L. S. Pedrotti, *Introduction to Optics*, 2nd ed. (Prentice-Hall International, 1993).
22. P. B. Johnson and R. W. Christy, "Optical constants of the noble metals," Phys. Rev. B **6**(12), 4370–4379 (1972).
23. A. Taflove and S. C. Hagness, *Computational Electrodynamics: The Finite-Difference Time-Domain Method*, 3rd ed. (Artech House, 2005).

1. Introduction

For several hundred years, the diffraction limits of optical lenses have restricted the sensitivity and resolution of optical, radio frequency, imaging, and sensing devices. In 1873, E. Abbe found that the diffraction limit of an optical lens was about half a wavelength [1], and recently, various techniques for achieving higher resolution have been presented, which include negative refractive index lenses [2, 3], near-field tips [4], plasmonic superlenses [5, 6], far-field hyperlenses [7], far-field time-reversal devices [8, 9], far-field high-resolution fluorescence image microscopy [10], planar subwavelength structures that induce convergence of the near field [11], and superoscillating focusing without evanescent waves [12]. R. Merlin *et al*. [11, 13, 14] proposed that evanescent waves could be used to shape the electric field by radiationless electromagnetic interference to obtain higher resolution. Evanescent wave contributions to the total electromagnetic field propagating through subwavelength apertures were studied by L. E. Helseth [15, 16]. Y. Fu *et al*. [17, 18, 19] found that silver Fresnel zone plate structures aided superfocusing at visible wavelengths. Evanescent field effects on the near field focusing properties of zone plates were discussed in [20]. A better understanding of the theory and design principles underlying high resolution focusing can improve the quality of images in applications such as microscopy, detection, sensing, imaging, lithography, etc.

2. Structure and simulation methods

Figure 1 shows a cartoon plot of a Fresnel zone plate with fourteen zones ($N = 14$). In our study, the Fresnel zone plate was considered to be a binary zone plate with a substrate of a given material in the odd-numbered zones and free space in the even-numbered zones. The radius of each zone in the investigated Fresnel zone plate can be calculated by $R_n = \sqrt{(f + \frac{n\lambda_0}{2})^2 - f^2}$ [21], where R_n is the radius of the n_{th} zone, n is the zone number, f is the focal distance, λ_0 is the incident light wavelength, and t is the slab thickness, as shown in Fig. 1.

By using the angular spectrum representation, the field solutions computed from Maxwell's equations can be considered as a superposition of propagating and evanescent waves with different amplitudes and propagation directions. The field $\hat{E}(k_x, k_y; z)$ in the k-domain for a specific plane, z, can be evaluated by taking the Fourier transform of the field $E(x, y, z)$, where x and y are the transverse directions in Cartesian coordinates and k_x and k_y are the corresponding spatial

#116967 - $15.00 USD Received 9 Sep 2009; accepted 24 Sep 2009; published 28 Sep 2009

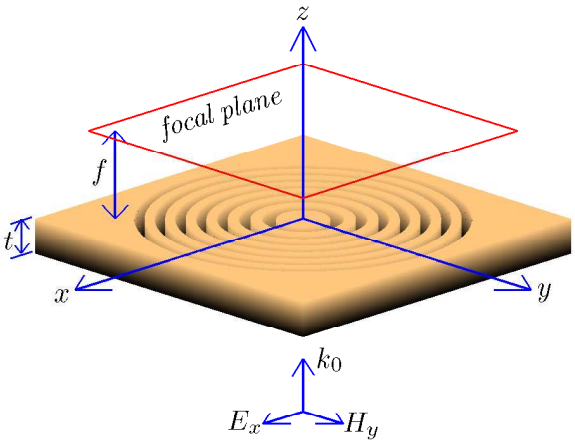

Fig. 1. A cartoon plot of the investigated Fresnel zone plate structure with fourteen zones ($N = 14$).

frequencies. This leads to the following equation:

$$\hat{E}(k_x,k_y;z) = \frac{1}{4\pi^2}\int_{-\infty}^{\infty}\int_{-\infty}^{\infty} E(x,y,z)e^{-i(k_x x+k_y y)}dxdy. \tag{1}$$

A wave occurring in the range of $k_x^2+k_y^2 \le k_0^2$ is classified as a propagating wave of the form $e^{i(k_x x+k_y y)}e^{\pm i|k_z|z}$, and it propagates along the $+z$ or $-z$ direction. Otherwise, the wave is evanescent and of the form $e^{i(k_x x+k_y y)}e^{-|k_z||z|}$, which decays exponentially along the z direction. Similarly, $E(x,y,z)$ can be obtained by taking the two-dimensional inverse Fourier transform of $\hat{E}(k_x,k_y;z)$,

$$E(x,y,z) = \int_{-\infty}^{\infty}\int_{-\infty}^{\infty} \hat{E}(k_x,k_y;z)e^{i(k_x x+k_y y)}dk_x dk_y. \tag{2}$$

Note that energy conservation relation must be satisfied, as dictated by

$$\int_{-\infty}^{\infty}\int_{-\infty}^{\infty} |E(x,y,z)|^2 dxdy = \int_{-\infty}^{\infty}\int_{-\infty}^{\infty} |\hat{E}(k_x,k_y;z)|^2 dk_x dk_y. \tag{3}$$

The propagating wave components of $E(x,y,z)$ can be obtained by taking the two-dimensional inverse Fourier transform of the components $k_x^2+k_y^2 \le k_0^2$ of $\hat{E}(k_x,k_y;z)$. The evanescent waves can also be obtained from the components $k_x^2+k_y^2 > k_0^2$ of $\hat{E}(k_x,k_y;z)$. Using Eq. (1)-(3), the physical properties of the propagating and evanescent waves in a specific plane, z, can be investigated.

3. Results and discussions

Two zone plates were investigated, with silver and glass in the odd-numbered zones and air in all of the even-numbered zones. All of the simulations used the finite-difference time-domain method. In the visible light region, silver has a negative dielectric constant, and the glass has a positive dielectric constant. The Drude model was used to model the dielectric constant of silver [22]. Perfectly matched layers were used to model infinite space [23]. In our simulation cases, the wavelength $\lambda_0 = 632.8$ nm, the focal distance $f = 1$ μm (or $1.58\lambda_0$), the slab thickness $t = 50$ nm, and an x-polarized incident plane wave with components E_x and H_y was considered, as shown in Fig. 1.

#116967 - $15.00 USD Received 9 Sep 2009; accepted 24 Sep 2009; published 28 Sep 2009

Figure 2(a) shows $|E_x(x,y)|$ in the focal plane of the silver Fresnel zone plate with $N = 14$. The predicted FWHMs (full width half maximums) of $|E_x(x,y)|$ were 414 nm ($0.654\lambda_0$) and 313 nm ($0.495\lambda_0$) in the x and y directions. Figure 2(b) shows $|\hat{E}_x(k_x,k_y)|$ plotted in the k-domain, which is the angular spectrum representation of Fig. 2(a). The incident wave was a plane wave propagating along the z direction, and it was identical to $k_x^2 + k_y^2 = 0$ in the k-domain. The propagating waves near $k_x^2 + k_y^2 \sim 0$ were larger in Fig. 2(b) because the incident plane wave $k_x^2 + k_y^2 = 0$ was diffracted by the zone plate structure. Notice that waves exist in $k_x^2 + k_y^2 \sim k_0^2$ regions of the circle, as shown in Fig. 2(b). These waves were also excited as the incident plane wave was diffracted by the structure. When $k_x^2 + k_y^2$ was slightly smaller than k_0^2, propagating waves with large propagating angles were found. For $k_x^2 + k_y^2$ values that were slightly larger than k_0^2, the waves were evanescent and had small decay coefficients. Because of the waves around the circle $k_x^2 + k_y^2 \sim k_0^2$, the field $|E_x(x,y)|$ had a smaller focal size, which is shown in Fig. 2(a). The angular spectrum representation in Fig. 2(b) shows more waves with $k_x^2 + k_y^2 \sim k_0^2$ along the k_y direction than the k_x direction, which allows the electric field $|E_x(x,y)|$ plotted in Fig. 2(a) to have a better focus in the y direction than the x direction.

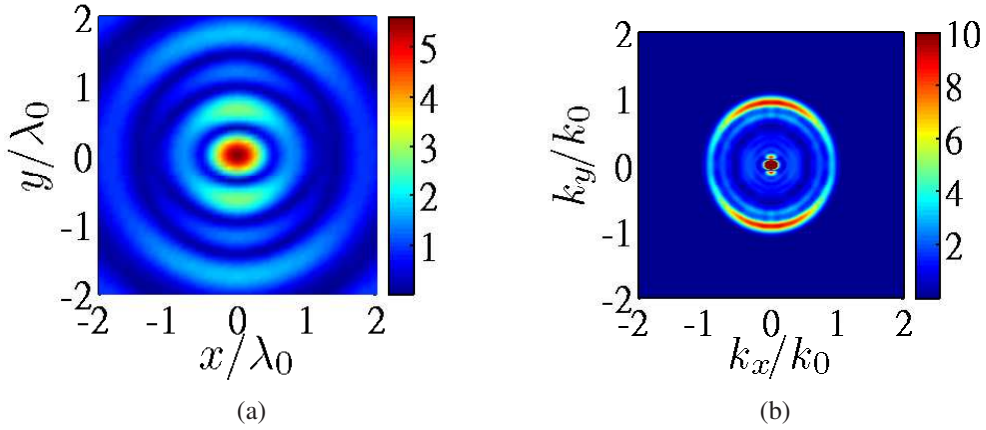

(a) (b)

Fig. 2. The predicted results for the silver Fresnel zone plate with $N = 14$: (a) $|E_x(x,y)|$ in the focal plane at $z = 1$ μm, and (b) $|\hat{E}_x(k_x,k_y)|$ the Fourier transform of (a). For better visualization, the scale for $|\hat{E}_x(k_x,k_y)|$ in (b) has been saturated at 10.

Figure 3 presents the results for a glass zone plate structure with the same shape as that plotted in Fig. 2. Figure 3(a) shows a plot of $|E_x(x,y)|$ in the focal plane, and Fig. 3(b) depicts $|\hat{E}_x(k_x,k_y)|$ in the k-domain. The FWHMs of $|E_x(x,y)|$ in the focal plane are 492 nm ($0.778\lambda_0$) and 396 nm ($0.626\lambda_0$) in the x and y directions. It is noted that $|\hat{E}_x(k_x,k_y)|$ near $k_x^2 + k_y^2 \sim k_0^2$ in Fig. 2(b) is larger than that in Fig. 3(b). This implies that there are more intense waves with $k_x^2 + k_y^2 \sim k_0^2$ in the focal plane of the silver zone plate than the glass zone plate. This explains why the focal size of silver zone plate in Fig. 2(a) is smaller than glass zone plate in Fig. 3(a); there are more high spatial frequency components in the focal plane for the silver zone plate.

By performing an inverse Fourier transform of the $k_x^2 + k_y^2 \leq k_0^2$ regions in Fig. 2(b) and Fig. 3(b), the components of the propagating waves can be obtained, which are shown in Fig. 2(a) and Fig. 3(a). Similarly, the components of the evanescent waves in Fig. 2(a) and Fig. 3(a) can be calculated in the regions of $k_x^2 + k_y^2 > k_0^2$ in Fig. 2(b) and Fig. 3(b). Figures 4(a) and (b) show the propagating waves and evanescent waves along the lines $y = 0$ and $x = 0$ in the focal planes of silver and glass Fresnel zone plates from Fig. 2 and Fig. 3. It was found

#116967 - $15.00 USD Received 9 Sep 2009; accepted 24 Sep 2009; published 28 Sep 2009

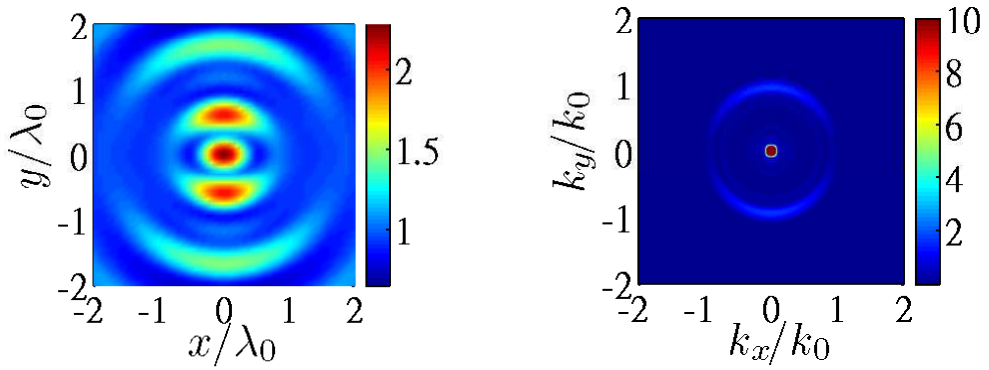

(a) (b)

Fig. 3. The predicted results for the glass Fresnel zone plate with $N = 14$: (a) $|E_x(x,y)|$ in the focal plane at $z = 1$ μm, and (b) $|\hat{E}_x(k_x,k_y)|$ the Fourier transform of (a). For better visualization, the scale for $|\hat{E}_x(k_x,k_y)|$ in (b) has been saturated at 10.

that the propagating waves for silver and glass zone plates are different. In contrast, the evanescent waves for these two zone plates are similar but smaller in magnitude than the propagating waves. Although the magnitudes of the evanescent waves are small, they can shape the propagating waves to help cause smaller focuses in silver and glass zone plates.

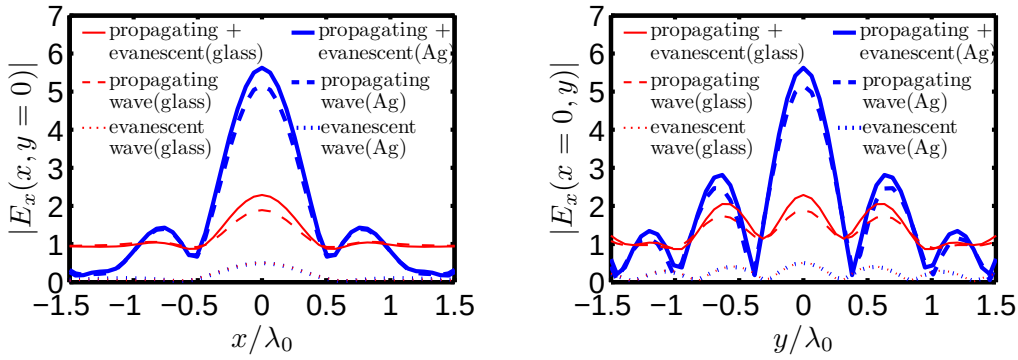

(a) (b)

Fig. 4. The predicted values of $|E_x(x,y)|$ for the propagating waves and evanescent waves along the lines (a) $y = 0$ and (b) $x = 0$ in the focal planes of silver and glass Fresnel zone plates.

Figure 5 shows a plot of $|\hat{E}_x(k_x,k_y)|$ at $z = 1$ μm (the focal plane) along the lines $k_y = 0$ and $k_x = 0$ for silver Fresnel zone plates with different numbers of zones, N, and for the glass Fresnel zone plate with $N = 14$. As the number of zones is increased in the silver Fresnel zone plate, more high spatial frequency components can be focused in the focal plane. Figure 5 shows that the silver Fresnel zone plate with $N = 6$ has larger spatial frequency components in comparison to those found in the glass Fresnel zone plate with $N = 14$. This means that a silver Fresnel zone plate can achieve a similar focal size as the glass Fresnel zone plate, but with fewer zones.

#116967 - $15.00 USD Received 9 Sep 2009; accepted 24 Sep 2009; published 28 Sep 2009

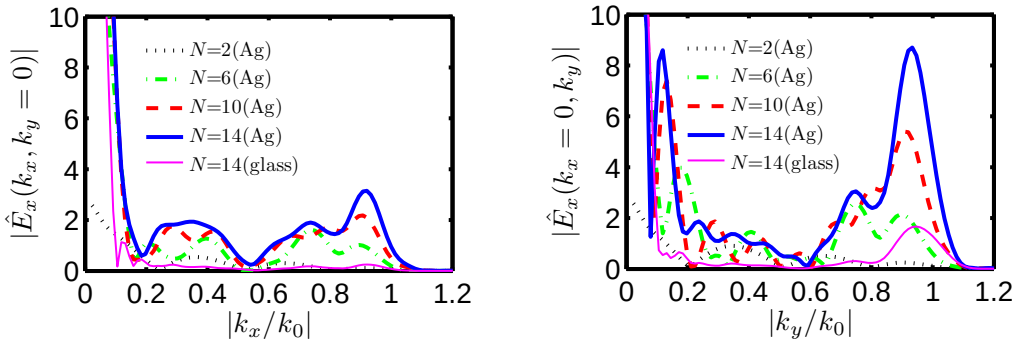

Fig. 5. The predicted values of $|\hat{E}_x(k_x,k_y)|$ along the lines (a) $k_y = 0$ and (b) $k_x = 0$ in the focal plane ($z = 1$ μm) for the Fresnel zone plates with different N values. The thick solid line is for the case in Fig. 2, and the thin solid line is for the case in Fig. 3.

From the previous discussions, it was noted that a better focus could be achieved as the components around circle $k_x^2 + k_y^2 \sim k_0^2$ are intensified. To understand how the components around the $k_x^2 + k_y^2 \sim k_0^2$ circle can shape the electric field, we show the normalized $|E_x(x, y = 0)|$ by taking the inverse Fourier transform of different combinations in the k-domain in Fig. 6. Here, we assume that all of the components in the k-domain are in-phase fields. Poor focusing was found for all fields inside the region of $0 \le k_x^2 + k_y^2 \le (0.1k_0)^2$ because these waves only contained low spatial frequency components. The field distribution for all waves inside the region of $0 \le k_x^2 + k_y^2 \le k_0^2$ is the diffraction-limited case. It is found that all fields in the regions of $(0.9k_0)^2 \le k_x^2 + k_y^2 \le k_0^2$ or $k_0^2 \le k_x^2 + k_y^2 \le (1.1k_0)^2$ can achieve better focusing than the diffraction-limited case, but the trade off is that the side lobes get larger and move closer to the main beams. If only 10% of the fields are comprised of waves around the $k_x^2 + k_y^2 \sim k_0^2$ circle ($(0.9k_0)^2 \le k_x^2 + k_y^2 \le k_0^2$ or $k_0^2 \le k_x^2 + k_y^2 \le (1.1k_0)^2$) and 90% are from the region of $0 \le k_x^2 + k_y^2 \le (0.1k_0)^2$, the focal sizes of the main beams are still smaller than the diffraction-limited case, and the side lobes get larger but move farther from the main beam. These predicted results could be useful as a guide in the design of the structures to recollect desired field components in the k-domain for small focal sizes and side lobe distributions.

4. Conclusion

We have shown the focusing properties of the silver and glass Fresnel zone plates using the finite-difference time-domain method and angular spectrum representation. It is found that the focal size varies when using different materials and different number of zones. The reason is that the evanescent waves and the higher spatial frequency components of the propagating waves diffracted by the zone plate structures can shape the electric field and obtain smaller focal sizes.

Acknowledgments

This work was supported by the National Science Council, Taiwan (NSC-96-2221-E-002-133-MY3, NSC-98-2120-M-002-004, NSC-98-2120-M-009-007), and the National Taiwan University Innovative Research Funds (NTU-98R0333). We are grateful to the National Center for High-Performance Computing, Taiwan, for the computer time and facilities.

#116967 - $15.00 USD Received 9 Sep 2009; accepted 24 Sep 2009; published 28 Sep 2009

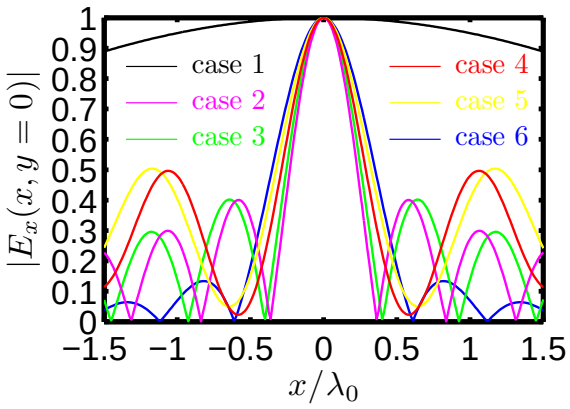

Fig. 6. The predicted values of normalized $|E_x(x, y = 0)|$ along the line $y = 0$ for different combinations of in-phase fields in the k-domain. These include case 1 (black line): $0 \leq k_x^2 + k_y^2 \leq (0.1k_0)^2$, case 2 (magenta line): $k_0^2 \leq k_x^2 + k_y^2 \leq (1.1k_0)^2$, case 3 (green line): $(0.9k_0)^2 \leq k_x^2 + k_y^2 \leq k_0^2$, case 4 (red line): 90% of case 1 and 10% of case 2, case 5 (yellow line): 90% of case 1 and 10% of case 3, and case 6 (blue line), which is the diffraction-limited case: $0 \leq k_x^2 + k_y^2 \leq k_0^2$.

#116967 - $15.00 USD Received 9 Sep 2009; accepted 24 Sep 2009; published 28 Sep 2009